Optimal rotary control of the cylinder wake using POD reduced order model

Bergmann M., Cordier L. & Brancher J.-P.

LEMTA, UMR 7563 (CNRS - INPL - UHP)
ENSEM - 2, avenue de la forêt de Haye
BP 160 - 54504 Vandoeuvre cedex
Michel.Bergmann@ensem.inpl-nancy.fr

Abstract

This article investigates the optimal control approach for the active control and drag optimization of incompressible viscous flow past cylinders. The control function is the time harmonic angular velocity of the rotating cylinder. The wake flow is solved in the laminar regime ($Re = 200$) with a finite element method. Due to the CPU and memory costs related to the optimal control theory, a *Proper Orthogonal Decomposition* (POD) Reduced Order Model (ROM) is used as the state equation. Since the POD basis represents only velocities, we minimize a drag-related cost function characteristic of the wake unsteadiness. The optimization problem is solved using Lagrange multipliers to enforce the constraints. 25% of relative drag reduction is found when the Navier-Stokes equations are controlled using the optimal control function determined with the POD ROM. A cost reduction factor of respectively one hundred and six hundred is obtained for respectively the CPU time and the memory. Finally, limits of the performance of our approach are discussed.

1 Introduction

Due to its simple geometry and its representative behaviour of separated flows [23], the viscous flow past a circular cylinder has been extensively used in the past decade as a testbed to develop methodologies that can be used later to control more complex flows. Different experimental or numerical approaches have been successfully employed for the control of a wake flow but recently optimal control theory attracted increased attention. For example, [13, 15, 19] used the optimal control theory with the two-dimensional Navier-Stokes equations as the state equation to control by rotary oscillation the unsteady wake of the cylinder. An attractive element of the optimal control approach is the introduction of a cost function which provides a quantitative measure of the desired objective. However the numerical costs (CPU and memory) associated with the adjoint equation-based methods used to solve these optimization problems are so important that the three-dimensional Navier-Stokes equations are rarely studied. For cutting down the numerical costs different approaches are possible (see [12] for a review). One promising approach is to first use reduced order models to approximate the fluid flow and then to optimize exactly the reduced models (read [1] for a discussion of the use of approximation models in optimization).

The main objective of this article is to develop a low-cost optimal control approach for drag minimization of the cylinder wake with harmonic rotary control for control function. This investigation of drag reduction by unsteady rotary oscillation of the cylinder was motivated in part by the experience of Tokumaru and Dimotakis [22] where 80% of relative drag reduction was empirically found ($Re = 15,000$). Recently, Protas and Wesfreid [20] show[1] that in the supercritical regime of the wake flow, the controllability increases with the Reynolds number. Therefore, since the wake flow remains two-dimensional up to a value of the Reynolds number approximately equal to 190 where a spanwise supercritical Hopf bifurcation occurs and where the three-dimensional effects appear [17, 3], the optimal value of the Reynolds number for our two-dimensional study is slightly lower than 200. However for facilitating the comparisons with the results of the literature, a Reynolds number of 200 is considered. Finally, for the reduced basis approach discussed above different basis functions exist: for example Lagrange basis, Hermite basis, Taylor basis, *Proper Orthogonal Decomposition* basis (POD),... According to the observations of He *et al.* [13], the control minimizing the drag generates vortices that are less energetic than those produced by the stationary cylinder. An energetic criterion seems to be well adapted to the investigation of drag reduction.

[1] The argumentation is quoted from [19]: "The mean flow consists of two contributions: the drag of the *basic flow* (i.e., the unstable, steady, symmetric flow) which at a given Reynolds number remains fixed and the drag of the *mean flow correction* which is due to the vortex shedding. As the Reynolds number increases, the relative contribution of the oscillatory part of the flow to drag becomes more significant." increasing the controllability of the flow.

Therefore, due to the energetic optimality of convergence of the POD basis [16, 6], POD is used to develop a POD Reduced Order Model (ROM) for the controlled cylinder. A similar approach was already done in [9, 10] to control the wake flow at a supercritical Reynolds number of 100.

This article is organized as follows: §2 introduces the flow configuration and describes the numerical method used to simulate the flow. In the next two sections, the *Proper Orthogonal Decomposition* is first introduced (§3), then we outline the *control function method* used to develop a POD ROM of the controlled flow (§4). The optimal control problem is stated in §5 which includes the definition of the cost function and a description of the Lagrange multiplier method used to solve the constrained optimization problem. Finally, before to present the results of the POD ROM based control in §6.2 and the drag reduction obtained with the Navier-Stokes equations when the optimal control function determined with the POD ROM is used (§6.3), we describe in §6.1 how to determine generalized POD basis functions.

2 Flow configuration

The flow around a circular cylinder of diameter D is solved on a two-dimensional domain Ω filled with a Newtonian incompressible viscous fluid (figure 1). The continuity and Navier-Stokes equations written in dimensionless form are discretized in time by a three steps projection method and in space using a Galerkin finite element approximation (P_1, P_1). The unstructured mesh consisting of $25,000$ triangles and $12,000$ vertices is refined around the cylinder and in the wake to capture the Von Kármán's street. The details of the numerical method can be found in [7] and will not be discussed here.

The simulations are performed at a Reynolds number equal to 200. One can notice on figure 2 that our numerical simulation exhibits the well-known Von Kármán street and that no spurious reflections from the downstream boundary are visible.

In a viscous flow the total forces acting on a body are contributed by the pressure and skin friction terms. Let K_p be the pressure coefficient defined by

$$K_p = \frac{P - P_\infty}{1/2\rho U_\infty^2}$$

where the subscript ∞ denotes quantities evaluated on the input boundary. The aerodynamic coefficients can then be calculated in a dimensionless form as:

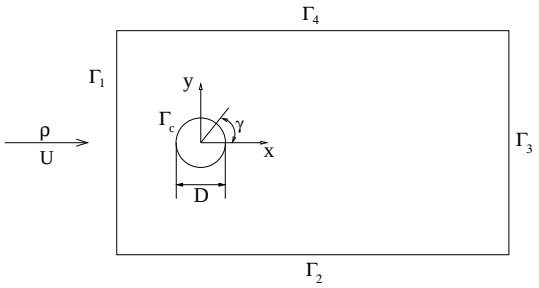

Figure 1: Geometry of the domain (diameter of the cylinder=1; upstream and downstream boundaries are respectively at 10 and 20 from the center of the cylinder; height=20).

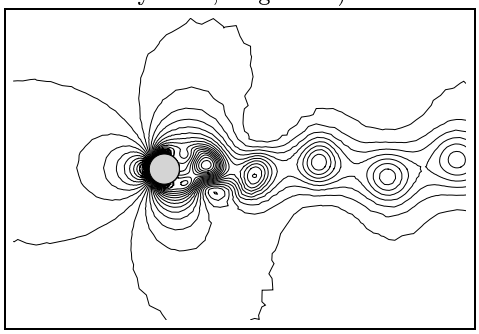

Figure 2: Pressure contours at $t = 150$ for $Re = 200$.

$$\begin{aligned} \boldsymbol{C} &= \boldsymbol{C}_p + \boldsymbol{C}_\nu = (C_D,\ C_L)^T \\ &= -\int_{\Gamma_c} K_p \boldsymbol{n}\, d\Gamma + \frac{2}{R_e}\int_{\Gamma_c} \frac{\partial \boldsymbol{u}}{\partial \boldsymbol{n}}\, d\Gamma. \end{aligned} \tag{1}$$

where C_D and C_L represent respectively the drag and lift coefficients.

The time histories of the lift and drag coefficients are represented in figure 3. Their time averaged amplitudes are respectively 0.0921 and 1.3822 (table 1). The periodic regime which is reached asymptotically, when the non linear saturation is observed, is characterized by the frequency at which vortices are shed. For comparison purposes, it was found convenient to introduce a non dimensional representation of the shedding frequency, the Strouhal number defined as

$$S_t = \frac{f\, D}{U_\infty}$$

where f is the fundamental frequency obtained by a spectral analysis of the aerodynamic coefficients (see figure 4).

In table 1, our vortex shedding Strouhal number and time-averaged drag coefficient are compared to reference results available in the literature. The agreement with all the previous experimental and computational data is very good. Similarly (not shown in table 1),

R_e	*Auteurs*	S_t	C_D
200	Braza *et al.*[5]	0.200	1.400
	Henderson *et al.*[14]	0.197	1.341
	He *et al.*[13]	0.198	1.356
	Homescu *et al.*[15]	-	1.440
	present study	**0.195**	**1.382**

Table 1: Comparison for $R_e = 200$ of the vortex shedding Strouhal number and the mean total drag coefficient for our simulation and reference results.

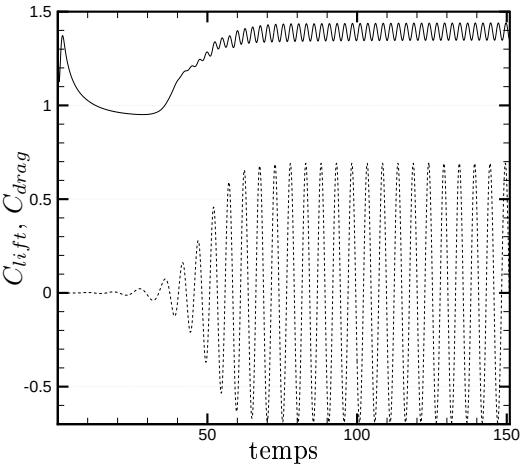

Figure 3: Temporal evolution of the aerodynamic coefficients for the stationary cylinder at $Re = 200$. $-$ drag, $\cdots$ lift.

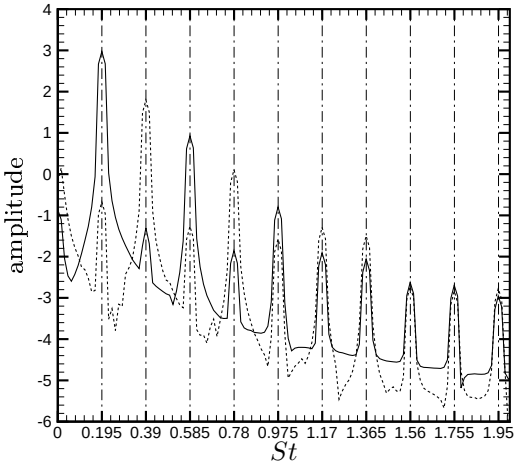

Figure 4: Power spectral density of the aerodynamic coefficients. $-$ drag, $\cdots$ lift.

the time-averaged lift coefficient is seen to be in very good agreement with the results obtained previously.

Therefore, for the low Reynolds number value of this study, our two-dimensional numerical simulation can be viewed to represent correctly the dynamics of the cylinder wake flow. However, we have to keep in mind that for higher values of the Reynolds number, the three dimensional phenomena become predominant explaining the well-known over-prediction of the drag coefficient for two-dimensional simulations (see [23]).

Hereafter, we consider that the cylinder rotates counterclockwise with angular velocity $\gamma(t)$ which is sought using the Optimal Control Theory in order to reduce the instationnarity of the wake.

3 Proper Orthogonal Decomposition (POD)

This method was introduced in turbulence by Lumley in 1967 [16] as an unbiased definition of the coherent structures widely known to exist in a turbulent flow. Starting with a set of realizations of the velocity fields $\boldsymbol{u}(\boldsymbol{X})$ where $\boldsymbol{X} = (\boldsymbol{x}, t) \in \mathcal{D} = \Omega \times \mathbb{R}^+$, a coherent structure is defined as the deterministic function $\boldsymbol{\Phi}(\boldsymbol{X})$ which is most similar on average to the realizations $\boldsymbol{u}(\boldsymbol{X})$. Mathematically, the notion of "most similar" corresponds to the solution of the following constrained maximization problem:

$$\max_{\boldsymbol{\Phi}} \langle |(\boldsymbol{u}, \boldsymbol{\Phi})|^2 \rangle \quad \text{w.r.t.} \quad \|\boldsymbol{\Phi}\|^2 = 1 \tag{2}$$

where $(.,.)$ denotes a scalar product in the Hilbert space of square-integrable functions, $|.|$ is the corresponding norm and the brackets $\langle . \rangle$ denote an averaging operation, which may be a time or space average. More details on POD and all the justifications can be found in [6].

From variational calculus it can be shown that the problem (2) is equivalent to a Fredholm integral eigenvalue problem:

$$\int_{\mathcal{D}} R_{ij}(\boldsymbol{X}, \boldsymbol{X'}) \Phi_j(\boldsymbol{X'})\, d\boldsymbol{X'} = \lambda \Phi_i(\boldsymbol{X}) \tag{3}$$

where $R_{ij}(\boldsymbol{X}, \boldsymbol{X'})$ is the two-point space-time correlation tensor. Since R is self-adjoint and non-negative definite, it follows from the Hilbert-Schmidt theory that equation (3) has a denumerable infinite number of eigenvalues $\lambda^{(n)}$ and eigenfunctions $\Phi_i^{(n)}$ ($n = 1, \ldots, +\infty$). These eigenvalues are all real and positive and form a decreasing and convergent series. The associated eigenvectors $\boldsymbol{\Phi}^{(n)}$ form a complete orthogonal set that is optimal in an energetic sense (for a given number of modes N, the projection on the subspace spanned by the N leading eigenfunctions will contain the greatest possible kinetic energy on average). Since

the POD eigenfunctions can be represented as linear combinations of the velocity fields, they inherit all the properties of the original data that are linear or homogeneous. Hence the eigenfunctions are divergence free for an incompressible fluid and verify automatically the homogeneous boundary conditions of the numerical simulation used to determine the flow realizations.

Depending on the choice made for the average operator $\langle . \rangle$ appearing in (2), two equivalent formulations of POD can be found [6]. When the average is estimated in time, the first approach called classical POD or direct method and originally introduced by Lumley is obtained. In this case, the kernel R of the Fredholm equation (3) is replaced by the two-point spatial correlation tensor $r_{ij}(\boldsymbol{x}, \boldsymbol{x'})$ and the eigenfunctions $\boldsymbol{\Phi}(\boldsymbol{X})$ by $\boldsymbol{\phi}(\boldsymbol{x})$. In the second case suggested by Sirovich [21] and called snapshot POD, the average operator is evaluated as a space average over the domain in interest. The Fredholm equation to be solved is then defined by:

$$\int_T C(t,t')a^{(n)}(t')\,dt' = \lambda^{(n)}a^{(n)}(t) \tag{4}$$

where $C(t,t') = \dfrac{1}{T}\displaystyle\int_\Omega u_i(\boldsymbol{x},t)u_i(\boldsymbol{x})\,d\boldsymbol{x}$ is the temporal correlation tensor.

For reasons of statistical convergence of the average operator, the snapshot POD is more appropriate when data issued from numerical simulations are used. Hence, this method was adopted in our work.

Finally the set of POD modes $\{\boldsymbol{\phi}^{(n)}\}_{n=1}^{+\infty}$ is complete in the sense that any velocity field $\boldsymbol{u}(\boldsymbol{x},t)$ can be expanded in the eigenfunctions as

$$u_i(\boldsymbol{x},t) = \sum_{n=1}^{N_{POD}} a^{(n)}(t)\phi_i^{(n)}(\boldsymbol{x}). \tag{5}$$

where N_{POD} is equal to the number of flow realizations used to solve the POD problem (4).

4 POD ROM of the controlled cylinder wake

When the rotary control is applied, the boundary conditions on the cylinder become inhomogeneous and time-dependent. As a consequence, the POD basis functions used in the Galerkin projection have not homogeneous boundary conditions and extra terms appear in the POD reduced order model. To address this situation, the *control function method* introduced in [9] is used. In this approach, the velocity expansion is now defined as

$$\boldsymbol{u}(\boldsymbol{x},t) = \boldsymbol{u}_m(\boldsymbol{x}) + \gamma(t)\,\boldsymbol{u}_c(\boldsymbol{x}) + \sum_{k=1}^{N_{POD}} a^{(k)}(t)\boldsymbol{\phi}^{(k)}(\boldsymbol{x}) \tag{6}$$

where $\boldsymbol{u}_m(\boldsymbol{x})$ is the mean velocity field obtained as an ensemble average of the flow realizations and where $\boldsymbol{u}_c(\boldsymbol{x})$ is an arbitrary control function satisfying homogeneous boundary conditions. A convenient way to generate it is to take the solution for the steady cylinder rotation with $\gamma = 1$.

The weak form of the Navier-Stokes equations is then restricted to the POD subspace $D_{N_{gal}}^{POD}$ spanned by the first N_{gal} spatial eigenfunctions $\boldsymbol{\phi}^{(i)}$. The energetic optimality of the POD basis functions suggests that only a very small number of POD modes may be necessary to describe efficiently any flow realizations of the input data. The dimension $N_{gal} \ll N_{POD}$ of the subspace $D_{N_{gal}}^{POD}$ is the smallest integer M such that the relative information content defined as the ratio $\sum_{i=1}^{M}\lambda^{(i)} / \sum_{i=1}^{N_{POD}}\lambda^{(i)}$ is greater than $\delta\%$ where δ is a predefined percentage of energy (here $\delta = 99$ and $M = N_{gal} = 4$ see figure 9). The Galerkin projection yields [7]:

$$\begin{aligned}\left(\boldsymbol{\phi}^{(i)},\, \frac{\partial \boldsymbol{u}}{\partial t} + (\boldsymbol{u}\cdot\boldsymbol{\nabla})\boldsymbol{u}\right) &= \left(p,\, \boldsymbol{\nabla}\cdot\boldsymbol{\phi}^{(i)}\right) - \left[p\,\boldsymbol{\phi}^{(i)}\right] \\ &- \frac{1}{Re}\left(\boldsymbol{\nabla}\boldsymbol{\phi}^{(i)},\, (\boldsymbol{\nabla}\boldsymbol{u})^T\right) + \frac{1}{Re}\left[(\boldsymbol{\nabla}\boldsymbol{u})^T\boldsymbol{\phi}^{(i)}\right]\end{aligned} \tag{7}$$

with $[\boldsymbol{a}] = \displaystyle\int_\Gamma \boldsymbol{a}\cdot\boldsymbol{n}\,d\Gamma$ and $(A,\,B) = \displaystyle\int_\Omega A : B\,d\Omega = \sum_{i,\,j}\int_\Omega A_{ij}B_{ji}\,d\Omega$.

Inserting the expansion (6) into the Galerkin projection (7) of the Navier-Stokes equations, we obtain after some algebraic manipulations the reduced order control model:

$$\begin{aligned}\frac{d\,a^{(i)}(t)}{d\,t} =& \mathcal{A}_i + \sum_{j=1}^{N_{gal}} \mathcal{B}_{ij}\,a^{(j)}(t) + \sum_{j=1}^{N_{gal}}\sum_{k=1}^{N_{gal}} \mathcal{C}_{ijk}\,a^{(j)}(t)a^{(k)}(t) \\ &+ \mathcal{D}_i\,\frac{d\,\gamma}{d\,t} + \left(\mathcal{E}_i + \sum_{j=1}^{N_{gal}} \mathcal{F}_{ij}\,a^{(j)}(t)\right)\gamma + \mathcal{G}_i\gamma^2\end{aligned} \tag{8}$$

The coefficients $\mathcal{A}_i$, $\mathcal{B}_{ij}$, $\mathcal{C}_{ijk}$, $\mathcal{D}_i$, $\mathcal{E}_i$, $\mathcal{F}_{ij}$ and $\mathcal{G}_i$ depend explicitly on $\boldsymbol{\phi}$, $\boldsymbol{u}_m$ and $\boldsymbol{u}_c$. Their expression are given in [6].

The system of equations (8) is then integrated in time with a fourth order Runge Kutta scheme from a given set of initial conditions

$$a^{(i)}(0) = (\boldsymbol{u}(\boldsymbol{x},\,0),\,\boldsymbol{\phi}^{(i)}(\boldsymbol{x})), \quad i = 1, \cdots, N_{gal} \tag{9}$$

yielding a set of predicted time histories for the mode

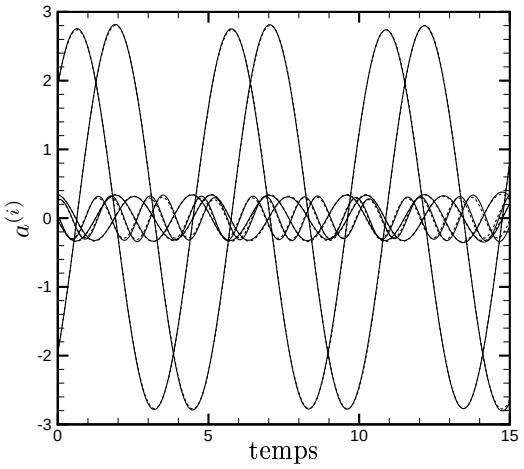

Figure 5: Comparison of the predicted ($-$) and projected ($\cdots$) mode amplitudes for the stationary cylinder ($\gamma = 0$).

amplitudes $a^{(i)}(t)$ which can be compared with the POD temporal eigenfunctions.

Due to the truncature involved in the POD-Galerkin approach, the higher POD modes corresponding to the dissipative scales of the flow are not explicitly taken into account in the POD ROM. As a consequence, when the equations (8) are integrated in time, numerical instabilities arise after a few vortex shedding period and the model is no longer sufficiently accurate. This problem is formally equivalent to that of large-eddy-simulation where we have to model the energy transfers between the Fourier modes lower than a given cutoff value that are simulated and those higher than this cutoff value that are not explicitly simulated. Here, the low-dimensional Galerkin model (8) is stabilized by an eddy-viscosity estimated as the solution of an auxiliary optimization problem described in [4].

As shown in figure 5 for an uncontrolled flow ($\gamma = 0$), when the POD ROM is stabilized numerically, excellent qualitative and quantitative agreement are found between the integrated time histories of the POD modes kept in the truncation and the results obtained by the numerical simulation. For a controlled flow, an accurate description of the dynamical behaviour is possible but special care is needed to develop the low-order model. This point is described in §6.

5 Optimal control approach

In this section we discuss how the Optimal Control approach can be used to determine the rotation rate $\gamma(t)$. The aim is to minimize a cost function $\mathcal{J}$, which incorporates the control goal and some measure of the control effort, over a certain period of time T corresponding to few periods of the Von Kármán street. Here we envisage employing the POD ROM of §4 for model-based control of the vortex shedding flow. Therefore, since only the flow velocities are directly represented by the POD basis functions, our objective is to minimize a drag-related cost function. A natural control aim is the reduction of the wake unsteadiness i.e. the energy of the wake [10]. Mathematically, this goal is expressed as the following functional

$$\begin{aligned}\mathcal{J}(\boldsymbol{u},\gamma(t)) &= \int_0^T \int_\Omega J(\boldsymbol{u}(\boldsymbol{x},\,t),\gamma(t))\,d\Omega dt \\ &= \frac{\alpha}{2}\int_0^T \int_\Omega \|\boldsymbol{u}(\boldsymbol{x},\,\boldsymbol{t})\|_2^2\,d\Omega dt + \frac{\beta}{2}\int_0^T \gamma(t)^2\,dt\end{aligned}$$

where the first term represents the control goal and the second a penalization term. In this formulation α and β are two positive regularization parameters that can be empirically chosen to limit the size of the control. Introducing the POD expansion (6), this functional becomes:

$$\begin{aligned}\mathcal{J}(\boldsymbol{a},\gamma(t)) &= \int_0^T J(\boldsymbol{a},\gamma(t))\,dt \\ &= \frac{\alpha}{2}\int_0^T \sum_{i=1}^{N_{gal}} {a^{(i)}}^2\,dt + \frac{\beta}{2}\int_0^T \gamma(t)^2\,dt.\end{aligned} \tag{10}$$

The flow control problem is then expressed as:

$$\begin{cases} \min\limits_{\gamma(t)} \mathcal{J}(\boldsymbol{a},\,\gamma(t)) \\ \quad \text{w.r.t.} \\ \mathcal{N}(\boldsymbol{a},\,\gamma(t)) = \boldsymbol{0}. \end{cases} \tag{11}$$

where the constraints $\boldsymbol{\mathcal{N}}(\boldsymbol{a},\,\gamma(t)) = \boldsymbol{0}$ correspond to the POD ROM (8).

The constrained optimization problem (11) is solved using the Lagrange multiplier method as described in [11]. The constraints are enforced by introducing the Lagrange multipliers or adjoint variables $\boldsymbol{\xi}$ and the Lagrangian functional

$$\begin{aligned}\mathcal{L}(\boldsymbol{a},\,\gamma,\,\boldsymbol{\xi}) &= \mathcal{J}(\boldsymbol{a},\gamma(t)) - \langle \boldsymbol{\xi},\,\boldsymbol{\mathcal{N}}(\boldsymbol{a},\,\gamma)\rangle \\ &= \mathcal{J}(\boldsymbol{a},\gamma(t)) - \sum_{i=1}^{N_{gal}} \int_0^T \xi_i(t)\,\mathcal{N}_i(\boldsymbol{a},\,\gamma)\,dt.\end{aligned} \tag{12}$$

The solutions (states $\boldsymbol{a}$, co-states $\boldsymbol{\xi}$ and control γ) of the new unconstrained optimization problem are such that $\mathcal{L}(\boldsymbol{a},\,\gamma,\,\boldsymbol{\xi})$ is rendered stationary:

$$\delta\mathcal{L} = \frac{\partial\mathcal{L}}{\partial a^{(i)}}\delta a^{(i)} + \frac{\partial\mathcal{L}}{\partial\gamma}\delta\gamma + \frac{\partial\mathcal{L}}{\partial\xi^{(i)}}\delta\xi^{(i)} \equiv 0.$$

where $\delta\boldsymbol{a}$, $\delta\gamma$ and $\delta\boldsymbol{\xi}$ are arbitrary variations.

Considering[2] that each argument of $\mathcal{L}$ is independent of the others, the optimality system is determined by setting the first variation of $\mathcal{L}$ with respect to $\boldsymbol{\xi}$, $\boldsymbol{a}$ and to γ to be equal to zero.

After evaluation the Fréchet differential $\dfrac{\partial \mathcal{L}}{\partial \xi^{(i)}}\delta\xi^{(i)}$ recovers the *state equation* $\boldsymbol{\mathcal{N}}(\boldsymbol{a},\,\gamma(t)) = \boldsymbol{0}$.

Setting the first variation of $\mathcal{L}$ with respect to the state $\boldsymbol{a}$ equal to zero gives, after integration by parts, the *adjoint equations*

$$\frac{d\,\xi^{(i)}(t)}{dt} = -\alpha a^{(i)}(t) - \sum_{j=1}^{N_{gal}} \left(\mathcal{B}_{ji} + \gamma(t)\,\mathcal{F}_{ji} + \sum_{k=1}^{N_{gal}} \left(\mathcal{C}_{jik} + \mathcal{C}_{jki}\right) a^{(k)}(t) \right) \xi^{(j)}(t) \tag{13}$$

with terminal conditions:

$$\xi^{(i)}(T) = 0. \tag{14}$$

Finally, setting the first variation of $\mathcal{L}$ with respect to the control γ equal to zero yields the optimality conditions

$$\delta\gamma(t) = -\sum_{i=1}^{N_{gal}} \mathcal{D}_i \frac{d\xi^{(i)}}{dt} + \beta\gamma + \sum_{i=1}^{N_{gal}} \left(\mathcal{E}_i + \sum_{j=1}^{N_{gal}} \mathcal{F}_{ij} a^{(j)} + 2\mathcal{G}_i\gamma(t) \right) \xi^{(i)}. \tag{15}$$

The first-order necessary conditions yield a system of coupled partial differential equations (state equation 8, adjoint equations 13 and optimality condition 15) called *optimality system*. Due to large storage and CPU costs that system cannot be solved without iteration. Instead a simple iterative process can be effected as follows:

Start with an initial guess for the control function $\gamma(t)$.

1. Using the latest guess for the control, solve the POD ROM (8) forward in time for the mode amplitudes $\boldsymbol{a}(t)$.
2. Using the mode amplitudes computed in step 1, solve the adjoint equations (13) backward in time for the adjoint variables $\boldsymbol{\xi}(t)$.
3. Using the state variables computed in step 1 and the adjoint variables computed in step 2, estimate the optimality condition (15).
4. Using this estimation compute a new guess for the control $\gamma_{\text{new}}(t) = \gamma_{\text{old}}(t) + \omega\, d$. Here d is a direction of descent estimated with one's favorite optimization method using the gradient of the functional $\frac{d\mathcal{J}}{d\gamma}$ and ω the length step in that direction.
5. If some stopping criterion is satisfied, stop; otherwise, return to step 1.

[2] This was not true for the original optimization problem (11) involving $\mathcal{J}$ since the arguments $\boldsymbol{a}$ and γ were constrained to satisfy $\boldsymbol{\mathcal{N}}(\boldsymbol{a},\,\gamma(t)) = \boldsymbol{0}$.

6 POD ROM based control

In §4, it was shown that the reduced order control model (8) can represent sufficiently well the dynamics of the vortex shedding flow. Therefore in this section, we use the results of the optimal control theory presented in §5 to determine a model based control function $\gamma(t)$.

6.1 Generalized POD basis functions

In this study we decide to not reset the POD low order model (8) during the optimization process. Clearly, it corresponds to the assumption that one must be able to predict the system behaviour during the period T of the optimization, hence the importance of developing accurate low order models. For this reason, we follow the method introduced in [9] and derived generalized POD basis functions. A slowly varying amplitude and frequency sinusoid or 'chirp' is imposed as rotation rate for the cylinder. This temporal excitation γ_e shown in figure 6 is mathematically represented by the function:

$$\gamma_e(t) = A_1 \sin(2\pi S_{t1}\, t) \times \sin(2\pi S_{t2}\, t - A_2 \sin(2\pi S_{t3}\, t))$$

where $A_1 = 4$, $A_2 = 18$, $S_{t1} = 1/120$, $S_{t2} = 1/3$ and $S_{t3} = 1/60$.

In figure 7 we show the spectra of the excitation function γ_e. The frequencies vary continuously from $S_t = 0$ to $S_t \simeq 0.65$ and the spectra presents a weak dominating mode for $S_t \simeq 0.4$.

The Navier-Stokes equations are then solved with γ_e for boundary conditions on the cylinder. During the course of the excitation 600 snapshots are taken uniformly over one period $T_e = 60$ of excitation. These snapshots are used to form the temporal correlation matrix for the Fredholm equation (4).

The POD eigenvalues for the uncontrolled flow ($\gamma = 0$) and manipulated flow ($\gamma = \gamma_e$) are shown in figure 8 on a semi log-scale. For the uncontrolled flow, the set

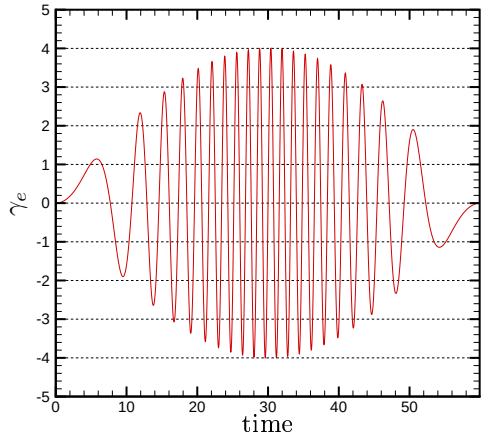

Figure 6: Temporal excitation γ_e imposed to the cylinder for deriving the generalized POD basis functions.

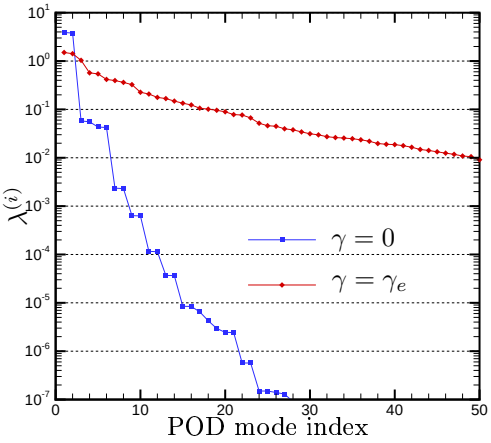

Figure 8: Comparison of the POD eigenvalue spectrum for the uncontrolled flow ($\gamma = 0$) and the manipulated flow ($\gamma = \gamma_e$).

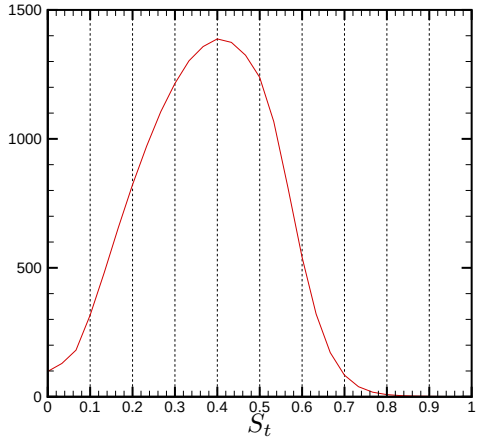

Figure 7: Spectra (in arbitrary units) of the temporal excitation γ_e.

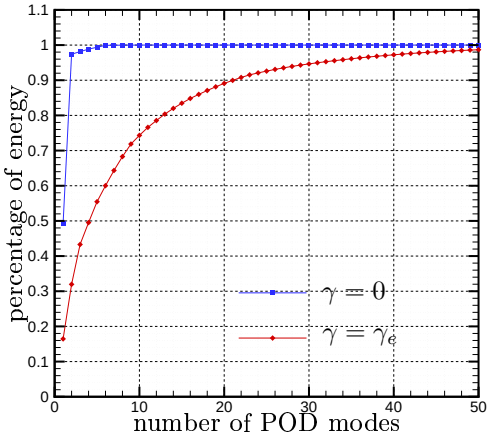

Figure 9: Comparison of the relative information content for the uncontrolled flow ($\gamma = 0$) and the manipulated flow ($\gamma = \gamma_e$).

of eigenvalues fall-off rapidly, and hence a low number of POD modes is necessary to represent accurately any velocity field. Clearly for the manipulated flow the spread of energy is much more uniform and many more degrees of freedom than for the uncontrolled flow are excited. As a consequence for a given number of modes kept in the POD expansion, the projection error of the snapshots on the POD basis functions is greater for the manipulated flow than for the uncontrolled flow. To make this idea more precise, one can study the relative information content as defined in §4. This quantity is represented in figure 9 for the uncontrolled flow ($\gamma = 0$) and manipulated flow ($\gamma = \gamma_e$). It is found that two modes are sufficient to represent 98% of the total kinetic energy in the uncontrolled case and that it is necessary to keep 40 modes (less than 7% of all the POD modes) when the excitation γ_e is applied. Therefore the state equation (8) used in the iterative optimization process of §5 correspond to $N_{gal} = 40$.

6.2 Results of the POD ROM based control

The results of this section correspond to the case when the cost of the control is neglected i.e. $\alpha = 1$ and $\beta = 0$ in the functional (10). The control function γ is determined as a converged solution of the iterative process introduced at the end of §5. As an initial guess for the control function the excitation γ_e is selected. In step 4 of the iterative method a steepest descent method is used in conjunction with a back-

tracking Armijo method[3] for the linear search. The details of this optimization method can be found in [18]. The iterative method is stopped when the last two values of the functional $\mathcal{J}$ is sufficiently close i.e. when $|\Delta\mathcal{J}(\boldsymbol{a},\gamma)| = |\mathcal{J}_{\text{new}}(\boldsymbol{a},\gamma) - \mathcal{J}_{\text{old}}(\boldsymbol{a},\gamma)| < 10^{-5}$. Once this criterion of convergence is reached, the relative reduction of the cost function $\mathcal{J}$ characterizing the wake unsteadiness is equal[4] to 43%. Finally the temporal evolution of the optimized control function γ_{opt} is shown in figure 10.

Reduction of the drag coefficient using time harmonic rotary oscillation was reported by [22, 2, 13, 15, 20]. Therefore, if we want to compare our result with those of the literature, we need to determine the amlitude A and the Strouhal number S_t such that the optimized control function writes $\gamma_{opt}(t) = A\sin(2\pi S_t t)$. A time average amplitude $A \simeq 2.2$ is easily determined. In figure 11 we show the spectra of the control function γ_{opt}: a mean peak appears corresponding to $S_t \simeq 0.53$ and two other peaks much less energetic are also clearly visible. According to [13] the contributions of these lower modes are negligible for the drag. As a consequence these peaks are neglected in the following and the optimal control γ_{opt} is sinusoidal with an amplitude $A = 2.2$ and a Strouhal number $S_t = 0.53$.

6.3 Drag reduction for the Navier-Stokes model

By definition of the optimization problem (11), the control function γ_{opt} is optimal for the POD ROM. There is no mathematical proof of optimality with respect to the Navier-Stokes model. If it was found that the optimized control function reduces the wake unsteadiness, the initial objective of this study is the optimal reduction of drag. Therefore it is necessary to solve the Navier-Stokes equations with a rotary control defined by $\gamma(t) = \gamma_{opt}(t)$ to determine the effect of this control function on the drag coefficient.

Figure 12 represents a comparison of the time evolution of drag of the uncontrolled ($\gamma = 0$, blue) and controlled ($\gamma = \gamma_{opt}$, green) flow. The drag reduction was found to be on the order of 25% (from approximately an average value of 1.4 to an average value of 1.04). In figure 13 we show the comparison of the variation versus time of the lift coefficient for the uncontrolled (blue) and controlled (green) flow. We observe that the amplitude of the lift oscillations is substantially reduced (from 1.38 to 0.34). These behaviour are synthesized in figure 14 where the polar curves (time evolution of the drag coefficient versus the lift coefficient) are represented for the uncontrolled (blue) and controlled (green) flow. The limit cycles appearing in this figure are well defined because each aerodynamic coefficient oscillates with one frequency. The power spectral density of the aerodynamic coefficients represented in figure 15 demonstrates that the controlled flow now oscillates at the frequency of the optimal control function ($S_t = 0.53$). Finally in figures 16a) and 16b) we show snapshots of the uncontrolled flow and of the optimally controlled flow (dashed lines represent negative vorticity). The significant vortex-shedding phenomenon observed in figure 16a) has been substantially reduced and the flow has been quasi-symmetrized. This is qualitatively similar to the effects observed by [22, 13].

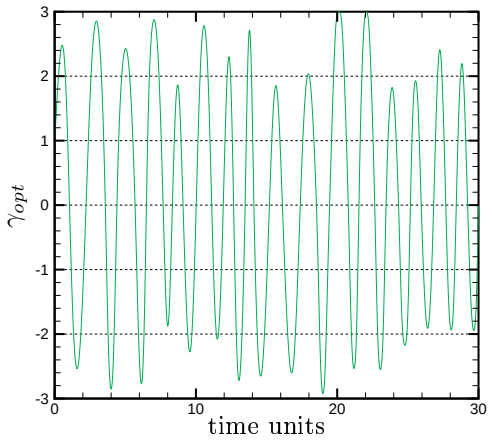

Figure 10: Time history of the optimized control function γ_{opt}.

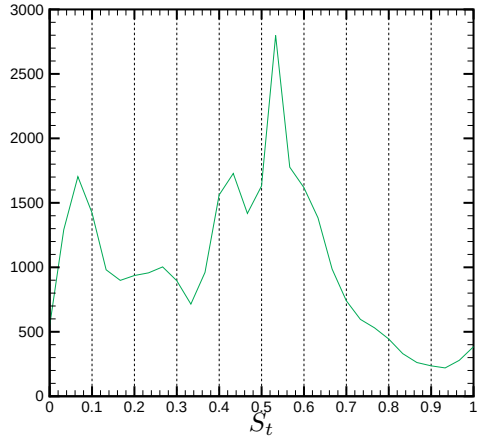

Figure 11: Spectra (in arbitrary units) of the optimized control function γ_{opt}.

6.4 Discussion

The numerical results obtained here with the POD ROM as state equation agree to a large extent to re-

[3] The step determined by the backtracking Armijo method is not too small and for this reason verifies the Goldstein condition [18].

[4] The value of $\mathcal{J}$ is 9.81 at the beginning of the iterative process and 5.63 when convergence is obtained. To be used as a reference value, $\mathcal{J}$ is approximately equal to 10 for an uncontrolled flow.

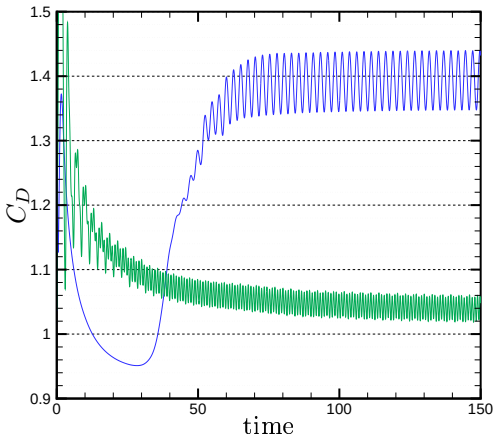

Figure 12: Comparison of the time evolution of drag of the uncontrolled (blue) and controlled (green) flow. Forcing was started at time $t = 0$.

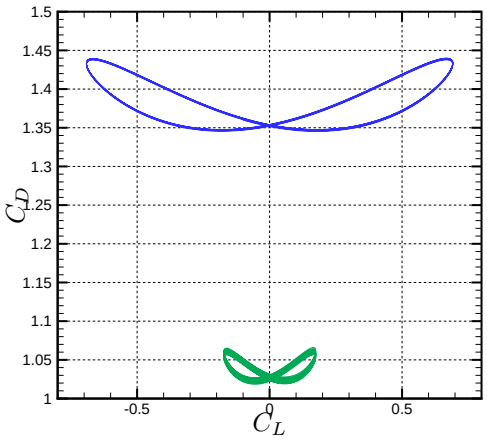

Figure 14: Polar curves: evolution of the drag coefficient versus the lift coefficient. In blue the uncontrolled flow and in green the controlled flow.

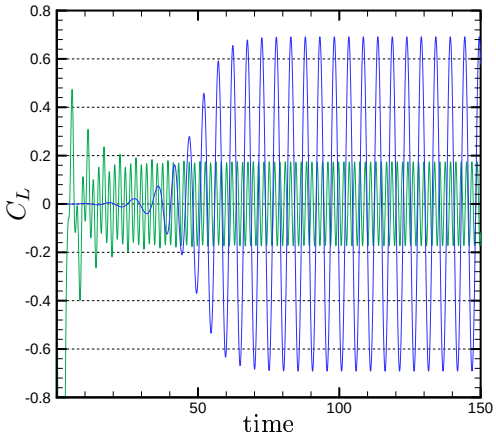

Figure 13: Comparison of the time evolution of lift of the uncontrolled (blue) and controlled (green) flow. Forcing was started at time $t = 0$.

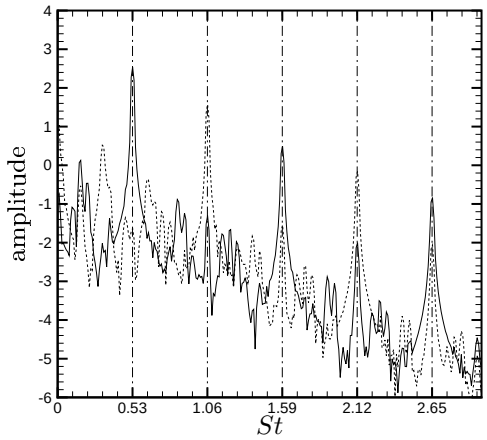

Figure 15: Power spectral density in log-scale of the aerodynamic coefficients for the controlled flow. – drag, $\cdots$ lift.

sults obtained in other numerical approach where the optimal control theory is applied for the same flow configuration to the Navier-Stokes equations. Protas and Wesfreid [19] obtain a drag reduction of about 15% for a Reynolds number equal to 150, presenting a less significant controllability. The research of He *et al.* [13] shows a 30% drag reduction if one uses a sinusoidal rotating cylinder with the amplitude $A = 3$ and the forcing Strouhal number $S_t = 0.75$. These optimal amplitude and forcing Strouhal number differ from the values found with our approach. As suggested by Homescu *et al.* in [15], these difference appear to be due to the formulation of the cost functionals used in our research and those in [13]. The objectives, while being physically identical, are mathematically different.

The drag reduction found with the Navier-Stokes equations as state equation is only slightly higher than the one found with our approach but the numerical costs (CPU and memory) associated to their control are much more important. Using a POD ROM the costs of the flow solves necessary at each iteration of the optimizer are greatly reduced. In our study, the CPU time necessary to obtain with the POD ROM the flow dynamics over one natural vortex shedding period represents 1% of the time necessary to solve the Navier-Stokes equations with the finite-element approach. In first approximation[5] the same gain is obtained for the

[5]Contrary to the Navier-Stokes equations, the adjoint and optimality equations are linear in the adjoint variables and hence easier to solve.

adjoint equations and the optimality conditions. The total CPU cost is thus drastically reduced (approximately a factor equal to one hundred). With regard to memory cost, note that we need to store the latest state approximation for all space-time to solve the adjoint equations and all the adjoint variables to estimate the optimality conditions. When the finite element simulation is used to solve the optimal control problem over a time horizon T_c, we need to store the state and adjoint variables (two velocity component and the pressure) at each time-step and for each vertice of the mesh. When the POD ROM is used, we only need to store the time evolution of the state variables $\mathbf{a}$ and of the adjoint variables $\boldsymbol{\xi}$ for N_{gal} POD modes plus the coefficients appearing in the state equation (8). The parameters used in this study are $T_c = 20$ for the time horizon (approximately four times the natural vortex shedding period), $\Delta t = 0.01$ for the time-step, $N_v = 12,000$ for the number of vertices and $N_{gal} = 40$ for the number of POD modes kept in the ROM. Here we found that the memory cost of the POD ROM approach is 600 times lesser than for the Navier-Stokes model. The reduction of the numerical costs offered by our approach is so important that the study of three-dimensional unsteady complew flows by the optimal control theory is now possible. However, as it was suggested by Gunzburger in [12], the success of our approach depends on the ability of the POD basis to well approximate the optimal solution and the path to the optimal solution. Using a POD ROM to solve an optimization problem in the extrapolary regime is not so clear. Certainly, some updating of the POD basis would be necessary during the optimization process like in the Trust Region POD method introduced by Fahl [8]. Theoretical work are still necessary to determine if the reduced order model approach is really useful in the flow optimization setting.

7 Conclusions

The objective of this study was to illustrate the potential gain that can be offered by the use of the Proper Orthogonal Decomposition for optimal control of fluid flows. Our methodology was presented for the unsteady rotary control of the cylinder wake in the laminar regime ($Re = 200$). Defining a cost function representative of the wake unsteadiness, the optimal control problem was solved with a POD ROM of the controlled flow as the state equation. The solution of the optimization process was then used to control numerically the wake flow with the Navier-Stokes equations as flow model. Finally, a significant reduction (25%) of the amplitude of the drag coefficient was found. These numerical results agree to a large extent to results obtained by other researchers [13, 15, 19] using the two-dimensional Navier-Stokes equations to solve the optimal control problem. Comparing to those studies, the main advantage of our approach is that the numerical costs (CPU and memory) are negligible (of the order of 1%). The conceptual drawback is that there is no mathematical assurance that the solution of the optimization algorithm working with the approximation models will correspond to the solution of the optimization problem for the original dynamical system. As it was suggested by Alexandrov *et al.* in [1], a possible way to be assured that the solution of the optimization problem for the reduced order model is likely to yield at least to a local optimum for the original high fidelity problem, is to use the general trust region framework[6]. Therefore are the POD ROM approach useful in the flow optimization setting ? A possible answer may be given by quoting Gunzburger [11] "without an inexpensive method for reducing the cost of flow computations, it is unlikely that the solution of optimization problems involving the three dimensional,

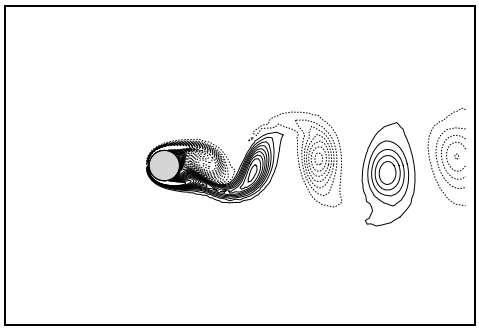

(a) Uncontrolled flow ($\gamma = 0$).

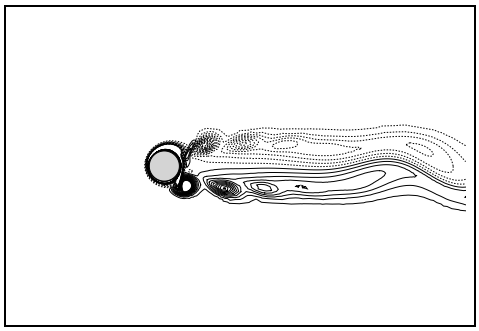

(b) Controlled flow $\gamma = \gamma_{opt}$.

Figure 16: Vorticity contour plot of the wake of the uncontrolled (a) and controlled (b) flow at $t = 150$.

[6] The trust region mechanism gives a measure of how well the approximation model is predicting improvement in the high-fidelity model and thus suggests criteria for automatically changing or improving the reduced model when poor or incorrect prediction of improvement is obtained. Fahl presents in [8] an algorithm that implements the combination of POD based reduced order modelling and trust region methods, the TRPOD (*Trust Region Proper Orthogonal Decomposition*).

unsteady Navier-Stokes system will become routine".

References

[1] Alexandrov N., Dennis Jr J.E., Lewis R.M. and Torczon V. (1997): A Trust Region framework for managing the use of approximation models in optimization. *Icase report*, N°. 97-50.

[2] Baek S.J. and Sung H.J. (1998): Numerical simulation of the flow behind a rotary oscillating circular cylinder. *Phys. Fluids*, **10** (4), pp. 869-876.

[3] Barkley D. and Henderson R.D. (1996): Three-dimensional Floquet stability analysis of the wake of a circular cylinder. *J. Fluid Mech.*, **322**, pp. 215-241.

[4] Bergmann M., Cordier L. and Brancher J.-P. (2003): Optimisation d'un modèle d'ordre réduit basé sur la Décomposition Orthogonale Aux Valeurs Propres. *LEMTA research report.*

[5] Braza M., Chassaing P. and Ha Minh H. (1986): Numerical study and physical analysis of the pressure and velocity fields in the near wake of a circular cylinder. *J. Fluid Mech.*, **165**, pp. 79-130.

[6] Cordier L. and Bergmann M. (2002a): Proper Orthogonal Decomposition: an overview. *Lecture Series 2002-04 and 2003-03* on post-processing of experimental and numerical data, Von Kármán Institute for Fluid Dynamics.

[7] Cordier L. and Bergmann M. (2002b): Two typical applications of POD: coherent structures eduction and reduced order modelling. *Lecture Series 2002-04 and 2003-03* on post-processing of experimental and numerical data, Von Kármán Institute for Fluid Dynamics.

[8] Fahl M. (2000): Trust-Region methods for flow control based on Reduced Order Modeling. *PhD dissertation, Trier university.*

[9] Graham W.R., Peraire J. and Tang K.T. (1999a): Optimal Control of Vortex Shedding Using Low Order Models. Part I. Open-Loop Model Development. *Int. J. for Numer. Meth. in Engrg.*, **44**(7), pp. 945-972.

[10] Graham W.R., Peraire J. and Tang K.T. (1999b): Optimal Control of Vortex Shedding Using Low Order Models. Part 2: Model-based control. *Int. J. for Numer. Meth. in Engrg.*, **44**(7), pp. 973-990.

[11] Gunzburger M. (1997): Lagrange multiplier techniques. *Lecture series 1997* on inverse design and optimization methods, Von Kármán Institute for Fluid Dynamics.

[12] Gunzburger M. (2000): Adjoint equation-based methods for control problems in incompressible, viscous flows. *Flow, Turbulence and Combustion*, **65**, pp. 249-272.

[13] He J.-W., Glowinski R., Metcalfe R., Nordlander A. and Périaux J. (2000): Active control and drag optimization for flow past a circular cylinder. Part 1. Oscillatory cylinder rotation. *J. Comp. Phys.*, **163**, pp. 83-117.

[14] Henderson R.D. (1997): Nonlinear dynamics and patterns in turbulent wake transition. *J. Fluid Mech.*, **352**, pp. 65-112.

[15] Homescu C., Navon I.M. and Li Z. (2002): Suppression of vortex shedding for flow around a circular cylinder using optimal control. *Int. J. Numer. Meth. Fluids*, **38**, pp. 43-69.

[16] Lumley J.L. (1967): The structure of inhomogeneous turbulence. *Atmospheric Turbulence and Wave Propagation*, ed. A.M. Yaglom & V.I. Tatarski, pp. 166-178.

[17] Noack B.R. and Eckelmann H. (1994): A global stability analysis of the steady and periodic cylinder wake. *J. Fluid Mech.*, **270**, pp. 297-330.

[18] Nocedal J. and Wright S.J. (1999): Numerical Optimization. *Springer series in operations research.*

[19] Protas B. and Styczek A. (2002): Optimal rotary control of the cylinder wake in the laminar regime. *Phys. Fluids*, **14** (7), pp. 2073-2087.

[20] Protas B. and Wesfreid J.E. (2002): Drag force in the open-loop control of the cylinder wake in the laminar regime. *Phys. Fluids*, **14** (2), pp. 810-826.

[21] Sirovich L. (1987): Turbulence and the dynamics of coherent structures. Part 1:Coherent structures. Quarterly of Applied Mathematics **XLV**, N° 3, pp. 561–571.

[22] Tokumaru P.T. and Dimotakis P.E. (1991): Rotary oscillatory control of a cylinder wake. *J. Fluid Mech.*, **224**, pp. 77-90.

[23] Williamson C.H.K. (1996): Vortex dynamics in the cylinder wake. *Annu. Rev. Fluid. Mech*, **28**, pp. 477-539.